Phase Diagram of Li−Mn−O Spinel in Air

J. M. Paulsen and J. R. Dahn*

Department of Physics, Dalhousie University, Halifax, Nova Scotia, B3H 3J5 Canada

Received February 12, 1999. Revised Manuscript Received August 23, 1999

Thermogravimetric analysis, solid electrolyte coulometry, and X-ray diffraction were used to examine the stable phases in the Li−Mn−O phase diagram. Our investigations concentrated on the equilibrium composition of the spinel phase in the system Li−Mn−O. Between 400 and 880 °C only spinel with the composition $Li_{1+x}Mn_{2-x}O_{4+\delta}$ ($\delta \approx 0$) is stable. The lithium stoichiometry, x, is a function of temperature, T, and oxygen partial pressure, $p(O_2)$. The value of x increases with decreasing temperature and increasing $p(O_2)$. The possible lithium stoichiometry range, Δx, at a given T and a given $p(O_2)$ is much smaller than generally accepted. We find that $0.05 < \Delta x < 0.13$. The spinel $Li_{1+x}Mn_{2-x}O_{4+\delta}$ has a negligible oxygen nonstoichiometric range, $\delta < 0.02$. Between 880 and 980 °C a variety of different tetragonal Li−Mn spinel phases $Li_{1-x}Mn_{2+x}O_4$ exist. Though commonly attributed as oxygen and lithium deficient spinel, our results indicate the absence of any significant oxygen deficiency. Below 400 °C spinel appears to be stable only as $Li_4Mn_5O_{12}$ and $LiMn_{1.75}O_4$. A phase diagram of the second kind is presented for the Li−Mn−O system (Figure 1).

Introduction

The most common cathode material for Li ion batteries is layered $LiCoO_2$. However, it would be preferable to avoid the toxic and expensive cobalt in commercial products. Therefore, lithium manganese spinel, $Li_{1+x}Mn_{2-x}O_4$, is under intense investigation as a possible replacement for the cobalt-based oxide.

Depending on preparation conditions, the equilibrium stoichiometry, x, of lithium in $Li_{1+x}Mn_{2-x}O_4$ can vary from $x = 0$ ($LiMn_2O_4$, stoichiometric spinel) to $x = 1/3$ ($Li_4Mn_5O_{12}$). The large stoichiometry range is possible since the mean oxidation state of manganese can vary from 3.5 when $x = 0$ to 4.0 in $Li_4Mn_5O_{12}$. [We are aware of the fact that the manganese oxidation state obtained from chemical analysis always is slightly smaller than 4.0 (approximately 3.9); see for example ref 1. We tried not to complicate the formulas, the obtained phase diagram, and the discussion, and hence, we generally dealt with the approximate, but more simple, formulas.]

Stoichiometric spinel has a reversible capacity of 145 (mA h)/g if all lithium can be removed. However, it exhibits poor cycling stability, especially at elevated temperatures (55 °C).[2] The cycling stability can be improved if cation-mixed spinel with $x > 0$ (typically $x \cong 0.08$) is used. Unfortunately the capacity decreases dramatically as x increases. Thus, there has been much work to prepare optimum materials from a capacity and cycling standpoint.

To prepare optimized materials, precise knowledge of the phase diagram is required. In this work the Li−Mn−O phase diagram in air is investigated (Figure 1). However, some features, such as the upper stability line of spinel (T_{c1}), are investigated over a wide range of oxygen partial pressure. Thermodynamic principles are explained which allow the extrapolation of the results to other oxygen pressures and temperatures. The oxygen stoichiometric range, δ, of the spinel phase was measured and was found to be negligible.

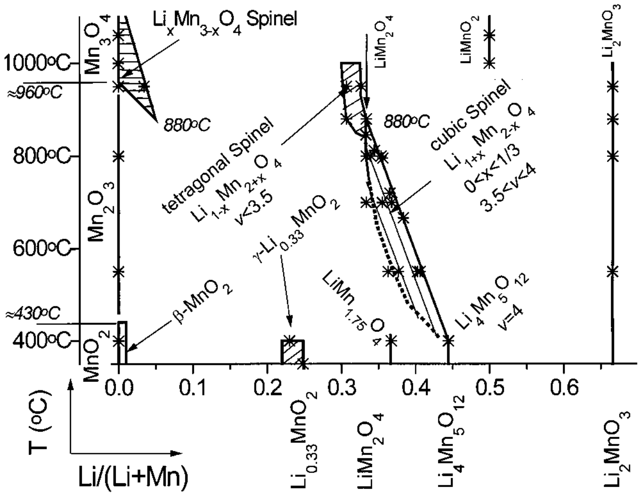

Figure 1. Phase diagram (of the second kind) of the system Li−Mn−O in air between 350 and 1060 °C. Li−Mn spinel exhibits several stability regions: $LiMn_{1.75}O_4$ and $Li_4Mn_5O_{12}$ (with Mn oxidation state $\nu = 4.0$) are stable below 400 °C; cation-mixed spinels $Li_{1+x}Mn_{2-x}O_4$ (with $3.5 < \nu < 4.0$) are stable at intermediary temperatures, and tetragonal $Li_{1-x}Mn_{2+x}O_4$ (with $\nu < 3.5$) is stable at elevated temperatures.

Cubic spinel has space group $Fd3m$ (no. 227). Mn is located on 16d sites. It is surrounded octahedrally by oxygen anions on 32e sites. Lithium is located on the 8a sites which are tetrahedrally surrounded by oxygen. Cation mixed spinel ($x > 0$) is made by replacing some of the Mn atoms in 16d by lithium atoms, designated by $Li[Li_xMn_{2-x}]O_4$. The spinels $Li[Li_xMn_{2-x}]O_4$ are equilibrium phases and must be distinguished from nonequilibrium phases such as $Li_xMn_2O_4$ (delithiated spinel)

---

(1) Ammundson, B.; Jones, D. J.; Roziere, J. *Chem. Mater.* **1996**, *8*, 2799.

(2) Blyr, A.; Sigala, C.; Amatucci, G.; Guyomard, D.; Chabre, Y.; Tarascon, J.-M. *J. Electrochem. Soc.* **1998**, *145*, 194.

10.1021/cm9900960 CCC: $18.00

Table 1. Overview of Spinel Phases[a]

name	formula	site/occupancy 8a (max 1)	site/occupancy 16d (max 2)	site/occupancy 32e(max 4)
	A: Thermodynamically Stable Phases			
stoichiometric	$LiMn_2O_4$ (c)	1Li	2Mn	4O
cation-mixed	$Li_{1+x}Mn_{2-x}O_4$ (c) ($0 < x \leq 1/3$)	1Li	xLi, $(2 - x)$Mn	4O
	$Li_4Mn_5O_{12}$	1Li	(1/3)Li, (5/3)Mn	
manganese-rich	$Li_{1-x}Mn_{2+x}O_4$ (t) ($0 < x < \sim 0.1$)	$(1 - x)$Li, xMn	2Mn	4O
	B: Thermodynamically Stable According to This Work			
manganese-deficient	$LiMn_{2-x}O_4$ (c) ($x = 1/4$)	1Li	1.75Mn	4O
	C: Thermodynamically Unstable. Preparation by Soft Chemical or Electrochemical Routes Only			
delithiated	$Li_{1-y}Mn_2O_4$	$(1 - y)$Li	2Mn	4O
lithiated	$Li_2Mn_2O_4$ (t)	2Li on 16c	2Mn	4O
	D: Phases Which Are Unstable According to This Work			
oxygen-deficient	$Li_{1+x}Mn_{2-x}O_{4-\delta}$ ($\delta \gg 0$)	1Li	xLi, $(1 - x)$Mn	$4 - \delta$
manganese-deficient	$LiMn_{2-x}O_4$ (c) ($0 < x < 1/4$)	1	$2 > x > 1.75$	4
oxygen-rich	$Li_2Mn_4O_9$ (c)	(8/9)Li	(16/9)Mn	4O
cation-deficient	$Li_{1-x}Mn_{2-y}O_4$ (c)	<1	<2	4O

[a] Abbreviations: (c) cubic, space group $Fd3m$; (t) tetragonal, space group $I4_1/amd$.

or $Li_2Mn_2O_4$ (lithiated spinel) which only can be obtained by soft chemical routes or electrochemical methods from $LiMn_2O_4$. Table 1 gives an overview of Li−Mn−oxide spinel phases.

Binary oxides AB_yO_x with B = transition metal and A = alkali or alkaline earth metal often show nonstoichiometry. The nonstoichiometry is possible because transition metals such as Mn are stable in different oxidation states. Manganese oxide is stable as MnO_2 at low temperatures in air. At higher temperatures or lower oxygen partial pressures first Mn_2O_3, then Mn_3O_4, and finally MnO are stable. Generally the mean Mn oxidation state increases with decreasing temperature and increasing $p(O_2)$. In the binary oxide $LiMn_2O_4$, this increase can, in principle, be achieved in two ways: by cationic mixing, $Li_{1+x}Mn_{2-x}O_4$, or by oxygen nonstoichiometry, $LiMn_2O_{4+\delta}$. If the ionic radii of the cations are a close match, cationic mixing can be expected and the oxygen nonstoichiometry which requires cationic or anionic vacancies would be largely suppressed.

The situation, however, is still more complicated in Li−Mn spinel. Besides oxygen nonstoichiometry and cation mixing, manganese deficiency could also be possible. To date, only cation mixing has been proven rigorously.[3] Lithium can substitute for tetravalent, octahedrally coordinated manganese on the 16d sites. Therefore, cation-mixed spinels $Li[Li_xMn_{2-x}]O_4$ are equilibrium phases. The equilibrium stoichiometry decreases from $x = 1/3$ at 400 °C to $x = 0$ (at $T \cong 880$ °C in air). The right panel of Figure 2 shows the simultaneous change of lattice constant which can be used to obtain the stoichiometry of cation-mixed spinel. At still higher temperatures, divalent manganese can substitute for lithium on tetrahedral sites, leading to thermodynamically stable (tetragonal) spinels with the composition $Li_{1-x}Mn_x[Mn]_2O_4$.[4] Manganese deficiency is possible since a replacement of manganese by a vacancy (instead of lithium) on octahedral positions (16d) still allows all lithium to remain on tetrahedral 8a sites. Therefore, manganese-deficient spinel $Li_1[Mn_{2-x}V_x]O_4$, where V is a Mn vacancy, could be an equilibrium phase, too. The possibility of large oxygen nonstoichiometry will be rejected in our work.

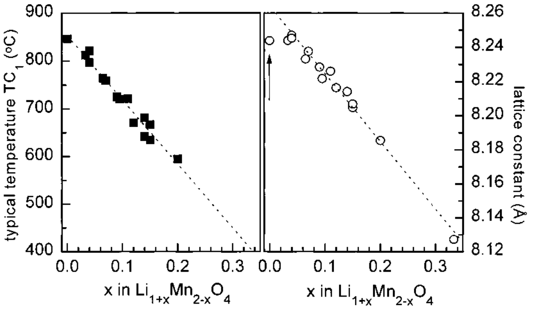

Figure 2. Properties of $Li[Li_xMn_{2-x}]O_4$ as a function of x. Data from ref 5. Left plot: Decomposition temperature T_{c1}. Right plot: Lattice constant.

During heating, a cation-mixed spinel $Li_{1+x}Mn_{2-x}O_4$ with large x decomposes into a spinel with smaller x and Li_2MnO_3 at a temperature called T_{c1}.[5] T_{c1} depends on the lithium stoichiometry, x, and $p(O_2)$. Thus, T_{c1} is the upper stability line of spinel with given composition x. The decomposition reaction is accompanied by an oxygen release that can be monitored by TGA. Below T_{c1} the mass is constant. A rapid oxygen release begins at T_{c1}; thus, the slope of the mass−temperature graph changes discontinuously at T_{c1}. Gao and Dahn suggested using the dependence of T_{c1} on x (shown in the left part of Figure 2) to measure the lithium stoichiometry in spinel.[3]

The opposite effect is also observed. Spinel with x near zero decomposes upon cooling to a spinel with larger x and manganese oxides. As an example, stoichiometric spinel ($x = 0$) decomposes very slowly at 400 °C. Endres et al. measured the change of the lattice constant of stoichiometric spinel that equilibrated for months at 400 °C in air.[6] The lattice constant decreased slowly with time, indicating an increase of x in the spinel phase.

Various publications deal with the oxygen stoichiometry of spinel; for example,[4,7,8] Hosoya et al. as well as

---

(3) Gao, Y.; Dahn, J. R. *Appl. Phys. Lett.* **1995**, *66*, 2487.

(4) Tarascon, J. M.; McKinnon, W. R.; Coowar, F.; Bowmer, T. N.; Amatucci, G.; Guyomard, D. *J. Electrochem. Soc.* **1994**, *141*, 1421.

(5) Gao, Y.; Dahn, J. R. *J. Electrochem. Soc.* **1996**, *143*, 1783.

(6) Endres, P.; Fuchs, B.; Kemmler-Sack, S.; Brandt, K.; Faust-Becker, G.; Praas, H.-W. *Solid State Ionics* **1996**, *89*, 221.

(7) Hosoya, M.; Ikuta, H.; Uchida, T.; Wakihara, M. *J. Electrochem. Soc.* **1997**, *144*, L52.

(8) Sugiyama, J.; Atsumi, T.; Hioki, T.; Noda, S.; Kamegashira, N. *J. Alloys Compds.* **1996**, *235*, 163.

Sugiyama et al. suggest large ranges of oxygen nonstoichiometry.[7,8] However, the models used by these authors are based on severe misinterpretation of the experimental data. During the TGA measurements the upper stability line, T_{c1} vs x, of spinel was crossed. These authors did not take into account that T_{c1} decreases with decreasing oxygen partial pressure as expected by a reaction, which is connected with an oxygen loss. This dependence of T_{c1} is known and was first measured by Yamada et al.[10] So the observed mass loss in refs 7 and 8 is not caused by an oxygen nonstoichiometry of the spinel phase but by the mass loss connected with the spinel decomposition reaction.

Gao and Dahn observed the occurrence of 3.3 and 4.6 V plateaus in the discharge and charge of some Li/$Li_{1+x}Mn_{2-x}O_4$ cells.[9] These plateaus had been attributed to manganese occupation of tetrahedral lithium sites. However, the Rietveld refinements of the presented data contradicted this assumption. Oxygen deficiency was suggested instead as the cause for the plateaus, without proof. Unfortunately, it is beyond the scope of this paper to correlate electrochemical data with oxygen stoichiometry.

Some publications describe the phase diagram of Li–Mn–O phases, for example, refs 3, 11, and 12. The results are usually displayed in ternary phase diagrams for a single temperature. A ternary diagram is suited to show the phase relations in a closed system with freely adjustable, but fixed, amounts of oxygen, lithium, and manganese. This is the case if a cathode in an electrochemical cell is charged at room temperature. A ternary diagram is not well suited to describe preparations at elevated temperatures. If the sample preparation is made in air, then the overall oxygen stoichiometry is not fixed. It depends on both temperature and oxygen partial pressure. Then thermodynamic relations and phase information are better displayed using a “phase diagram of the second kind”, which also can be called a “pseudobinary phase diagram”.[13] We describe the basic thermodynamics of such diagrams here.

If phase diagrams are investigated, then equilibrium thermodynamics and kinetic influences must be clearly distinguished. V. Massarotti et al., for example, state “XRD measurements proved the coexistence of spinel, lithium rich spinel and rock-salt phases in the Li–Mn–O system”.[14] However, according to the Gibbs phase rule in the general case, only two phases can coexist if $p(O_2)$ and T are fixed as we will show below. Kinetic effects may have influenced the results and must be considered. Basic thermodynamic considerations will be reviewed to avoid misinterpretation of experimental results.

The Li–Mn–O system is rather reactive at elevated temperatures ($T > 800$ °C), so quenching is necessary to freeze the high-temperature phase configuration. At temperatures above 1000 °C the reaction kinetics are so fast that quenching could not freeze the equilibrium configuration. By contrast, at temperatures below 400 °C equilibration occurs very slowly. Here typical equilibration times are weeks to months. Here, distinction between thermodynamics and kinetics is difficult, so the portion of the phase diagram (Figure 1) below 450 °C is less certain than the portion above 450 °C.

This work presents new experimental results to show that the oxygen nonstoichiometric range in the spinel phase is small, and to elucidate the phase diagram. Prior work is used as is relevant in the construction of the phase diagram.

Theoretical Considerations

Gibbs Phase Rule. The number of phases that can coexist in thermodynamic equilibrium is defined by the Gibbs phase rule.

$$F = K + 2 - P \tag{1}$$

In the case of Li–Mn–O it connects the number of components ($K = 3$), the number of phases in equilibrium (P), and the number free thermodynamic variables F (i.e., temperature and pressure). Assume that two free thermodynamic variables, temperature and total pressure, can be chosen freely; then the Gibbs rule predicts three coexisting phases. The equilibrium phase configuration is this configuration of all possible configurations, which gives the minimum free energy:

$$G(T,p,N_i) = N_1\mu_1(T,p) + N_2\mu_2(T,p) + N_3\mu_3(T,p) \Rightarrow \min \tag{2}$$

In this formula μ_i is the chemical potential of the ith component, which is the same in all coexisting phases, and N_i is the number of moles of the ith component.

In practice, measured amounts of lithium (i.e., carbonate) and manganese (i.e., oxide) are taken, and a solid-state reaction is performed. A measured amount of oxygen is not taken. During the reaction the oxygen stoichiometry of the sample equilibrates with the oxygen partial pressure of the gas phase at the given temperature. Therefore, it is meaningless to deal with oxygen as a free adjustable component. The component oxygen must be expressed by the corresponding chemical potential. This is made by applying a Legendre transformation onto G in eq 2. Therefore, the old free enthalpy, a function of temperature, pressure, and the amounts of the three components, is replaced by a new free enthalpy, $\tilde{G}$, a function of temperature, pressure, oxygen partial pressure, and the amounts of only two components. The amount of the third component (oxygen) is replaced by its chemical potential μ_3.

$$G(T,p,N_1,N_2,N_3) \Rightarrow \tilde{G}(T,p,\mu_3,N_1,N_2) = G(T,p,N_1,N_2,N_3) - N_3\mu_3$$

$$\tilde{G}(T,p,\mu_3,N_1,N_2) = N_1\mu_1(T,p,\mu_3) + N_2\mu_2(T,p,\mu_3) \Rightarrow \min \tag{3}$$

$$\mu_3 = (1/2)RT\ln(p(O_2))$$

---

(9) Gao, Y.; Dahn, J. R. *J. Electrochem. Soc.* **1996**, *143*, 100.

(10) Yamada, A.; Miura, K.; Hinokuma, K.; Tanaka, M. *J. Electrochem. Soc.* **1995**, *142*, 2149.

(11) Thackeray, M. M.; Mansuetto, M. F.; Dees, D. W.; Vissers, D. R. *Mater. Res. Bull.* **1996**, *31*, 133.

(12) Xia, Y.; Yoshio, M. *J. Electrochem. Soc.* **1997**, *144*, 2592.

(13) Pelton, A. D.; Schmalzried, H. *Metall. Trans.* **1973**, *4*, 1395. See also: Schmalzreid, H. *Ber. Bunsen-Ges. Phys. Chem.* **1984**, *88*, 1186.

(14) Massarotti, V.; Capsoni, D.; Bini, M.; Chiodelli, G.; Azzoni, C. B.; Mozzati, M. C.; Paleari, A. *J. Solid State Chem.* **1997**, *131*, 94.

The chemical potential of oxygen can be chosen freely by changing the oxygen partial pressure $p(O_2)$ of the gas phase. Temperature and total pressure can be chosen freely as well. This gives three free variables (T, p, $p(O_2)$). According to the Gibbs phase rule, two thermodynamic phases coexist in equilibrium, allowing one to display the phase relations of the Li−Mn−O system as a binary phase diagram. The x axis is the cationic composition, x = Li:(Li + Mn). The y axis is the temperature, or the oxygen partial pressure. This type of phase diagram is called a phase diagram of the second kind or a pseudobinary phase diagram.

Though generally two coexisting phases will be observed, in special cases three phases may coexist. Near the transition temperature T_{trans} of one equilibrium phase configuration to another equilibrium configuration, the driving force, ΔG, becomes small and vanishes at T_{trans}. [In the Gibbs phase rule this corresponds to a fixing of the temperature (only two free parameters remain), and three equilibrium phases are allowed.] In practice (especially if the temperature is low) three phases may coexist if the temperature is near the upper or lower stability limit of one of the phases.

Isovalent Lines in a ln(p(O_2))−(1/T) Plot. A binary phase diagram can be displayed in different forms. If it deals with nonstoichiometric phases, then a $p(O_2)-T-x$ diagram is appropriate. Such a diagram gives information about the equilibrium composition, x, of a phase depending on the equilibrium conditions T and $p(O_2)$. The variable x could represent the oxygen stoichiometry as well as a cationic stoichiometry range. An especially appropriate form to display the $p(O_2)-T-x$ relations are isovalent lines in a $\ln(p(O_2))-(1/T)$ plot.

A nonstoichiometric oxide releases oxygen if heated or if $p(O_2)$ is lowered:

$$LiMn_2O_4 = LiMn_2O_{4-\delta} + (\delta/2)O_2, \quad \Delta H = H(\delta), \quad \Delta S = \delta S_0 \quad (4A)$$

Alternately a cation nonstoichiometric oxide can decompose (thereby changing the cationic stoichiometry) and release oxygen:

$$Li_{1+x}Mn_{2-x}O_4 = (1 - x)LiMn_2O_4 + xLi_2MnO_3 + (x/2)O_2, \quad \Delta H = H(x), \quad \Delta S = xS_0 \quad (4B)$$

[Equations 4A and 4B are simplified. The more general but similar equations are $Li_{1+a}Mn_{2-a}O_{4+b} \Rightarrow Li_{1+a}Mn_{2-a}O_{4+b-\delta} + (\delta/2)O_2$ and $Li_{1+a}Mn_{2-a}O_4 \Rightarrow ALi_{1+a-x}Mn_{2-a+x}O_4 + BLi_2MnO_3 + (C/2)O_2$, respectively.]

The oxygen release after an increase of temperature or a decrease of oxygen partial pressure is caused by the entropy term $T\Delta S$. This term becomes larger with increasing temperature or decreasing oxygen partial pressure. The reaction entropy ΔS ($\Delta S > 0$) is caused mostly by the much larger entropy of oxygen in the gas phase ($S_0 = S(\text{gas}) - S(\text{solid})$). The equilibrium compositions, δ or x, are given by the minimum of the free energy of reaction $\Delta G = \Delta H - T\Delta S$. The enthalpy change ΔH is the change of the formation enthalpy of the solid phases.

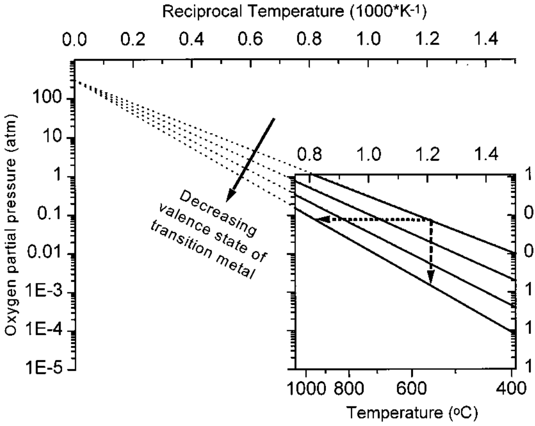

Figure 3. $p(O_2)-T-x$ diagram of a nonstoichiometric oxide in the form of isovalent lines in a $\ln(p(O_2))-(1/T)$ plot. The highlighted region gives the temperature and $p(O_2)$ range which is of interest here.

For reaction 4A a reaction constant, K, can be introduced

$$K = \frac{a(LiMn_2O_{4-\delta})(p(O_2))^{\delta/2}}{a(LiMn_2O_4)} \quad (5A)$$

with activities a. The corresponding equation (5B) derived from eq 4A would have the same form. The activities of solids, a, equal unity, and using the Gibbs−Helmhotz equation ($-RT \ln K = \Delta G$) yield

$$-\Delta G = -\Delta H + T\Delta S = RT(\delta/2) \ln p(O_2) \quad (6A)$$

and

$$-\Delta G = -\Delta H + T\Delta S = RT(x/2) \ln p(O_2) \quad (6B)$$

respectively. These are similar for both oxygen nonstoichiometry and for cation nonstoichiometry. Notice that these equations can both be transformed to a linear form, $y = A + Bx$

$$\ln p(O_2) = \frac{2\Delta S}{\delta R} - \frac{2\Delta H}{\delta R}\frac{1}{T} \quad (7)$$

From this it follows that the logarithm of $p(O_2)$ as a function of the reciprocal temperature is a straight line for every oxygen stoichiometry δ (the same is true for each cationic stoichiometry x). [The dependence of ΔH on temperature is neglected (Ullrich approximation).] Thus, the linear eq 7 can be displayed as a set of isostoichiometric straight lines in a $\ln(p(O_2))-(1/T)$ diagram. The mean Mn oxidation state is fixed on an isostoichiometric line. Now the oxygen release of an oxygen nonstoichiometric or a cationic nonstoichiometric oxide after heating or lowering $p(O_2)$ can be interpreted similarly. Both processes are driven by the desire of the manganese to decrease its mean oxidation state.

Figure 3 gives a typical schematic example for the thermodynamics of a nonstoichiometric oxide (either for oxygen or cationic nonstoichiometry) in the $\ln(p(O_2))-(1/T)$ diagram. The range of interest here (T = 400−1100 °C) is displayed as a cut of the diagram. A temperature increase (dotted arrow) leads to effects similar to those of a partial pressure lowering (dashed arrow). This allows one to predict phase relations if the

Table 2. Stoichiometry, Phase Composition, and Structure of the Li−Mn−O Samples[a]

T (°C)	no.	Li:Mn	phases	remark
350	A350	0.37:1	$Li_{0.33}MnO_2$ (γ) + $Li_4Mn_5O_{12}$	
400	A400	4:5	$Li_4Mn_5O_{12}$ (cs)	
	B400	3.5:5.5	$Li_4Mn_5O_{12}$ (cs)	
	C400	1:2	$Li_{1.1}Mn_{1.9}O_{4.35}$ (cs) + $Li_{0.3}MnO_2$ (γ)	
	D400	2.5:6.5	$Li_{1.1}Mn_{1.9}O_{4.35}$ (cs) + $Li_{0.3}MnO_2$ (γ) + MnO_2 (β)	near three phase equilibrium
	E400	2:7	$Li_{1.1}Mn_{1.9}O_{4.35}$ (cs) + $Li_{0.3}MnO_2$ (γ) + MnO_2 (β)	
	F400	1:5	$Li_{1.1}Mn_{1.9}O_{4.35}$ (cs) + $Li_{0.3}MnO_2$ (γ) + MnO_2 (β)	
	G400	0	MnO_2 (β)	
550	A550	1.5:2	$Li_{1+x}Mn_{2-x}O_4$ (cs) + Li_2MnO_3	$x \cong 0.22$
	B550	1.23:2	$Li_{1+x}Mn_{2-x}O_4$ (cs)	$x \cong 0.14$
	C550	1:2	$Li_4Mn_5O_{12}$ (cs) + Mn_2O_3	$x \cong 0.08$; equilibrium not reached; x still decreases
	D550	0.5:2	$Li_4Mn_5O_{12}$ (cs) + Mn_2O_3	
	E550	0.2:2	$Li_4Mn_5O_{12}$ (cs)+ Mn_2O_3	
	F550	0.1:2	$Li_4Mn_5O_{12}$ (cs) + Mn_2O_3	
	G550	0	Mn_2O_3	
550	acet550	1:2	$Li_{1+x}Mn_{2-x}O_4$ (cs) + Mn_2O_3	$x \cong 0.09$
790	stoi790	1:2	$Li_1Mn_2O_4$ (cs)	
800	A800	1.22:2	$Li_{1+x}Mn_{2-x}O_4$ (cs) + Li_2MnO_3	$x \cong 0.06$
	B800	1:2	$Li_1Mn_2O_4$ (cs)	$x \cong 0$
	C800	0.8:2	$Li_1Mn_2O_4$ (cs) + Mn_2O_3	
	D800	0.5:2	$Li_1Mn_2O_4$ (cs) + Mn_2O_3	
	E800	0.2:2	$Li_1Mn_2O_4$ (cs) + Mn_2O_3	
	F800	0.1:2	$Li_1Mn_2O_4$ (cs) + Mn_2O_3	
	G800	0	Mn_2O_3	
880	A880	1.25:2	$Li_1Mn_2O_4$ (cs) + Li_2MnO_3	$x \cong 0.0$
	B880	1:2	$Li_1Mn_2O_4$ (cs)	
	C880	0.8:2	$Li_{1-z}Mn_{2+z}O_4$ (ts) + $Li_yMn_{3-y}O_4$	
	D880	0.5:2	$Li_{1-z}Mn_{2+z}O_4$ (ts) + $Li_yMn_{3-y}O_4$ (s)	$z \cong 0.1$
	E880	0.2:2	$Li_{1-z}Mn_{2+z}O_4$ (ts) + Mn_2O_3 + $Li_yMn_{3-y}O_4$ (s)	
	F880	0.1:2	$Li_{1-z}Mn_{2+z}O_4$ (ts) + Mn_2O_3	
	G880	0	Mn_2O_3	
940	A940	1.25:2	$Li_{1-z}Mn_{2+z}O_4$ (cs) + Li_2MnO_3	$z \cong 0$
	B940	1:2	$Li_{1-z}Mn_{2+z}O_4$ (cs)	$0 < z < 0.1$
	C940	0.8:2	$Li_{1-z}Mn_{2+z}O_4$ (ts) +$Li_yMn_{3-y}O_4$ (s)	
	D940	0.5:2	$Li_{1-z}Mn_{2+z}O_4$ (ts) + $Li_yMn_{3-y}O_4$ (s)	$z \cong 0.1$, $y \cong 0.1$
	E940	0.2:2	$Li_{1-z}Mn_{2+z}O_4$ (ts) + $Li_yMn_{3-y}O_4$ (s)	
	F940	0.1:2	$Li_{1-z}Mn_{2+z}O_4$ (ts) + $Li_yMn_{3-y}O_4$ (s)	
	G940	0	Mn_2O_3	
890	T890	1.05:1.95	$Li_{1-z}Mn_{2+z}O_4$ (ts) + Li_2MnO_3	$z \cong 0.05$
920	T920	1.05:1.95	$Li_{1-z}Mn_{2+z}O_{4-\delta}$ (ts-compressed) + Li_2MnO_3	$z \cong 0.05$
950	T950	1.05:1.95	$Li_{1-z}Mn_{2+z}O_{4-\delta}$ (ts-stretched) + $LiMnO_2$	$z > 0.05$
980	T980	1.05:1.95	$Li_{1-z}Mn_{2+z}O_{4-\delta}$ (ts) + $LiMnO_2$ (o)	
1000	T1000	1:2	$LiMnO_2$ (o) + $Li_yMn_{3-y}O_4$ (s) + $LiMn_2O_4$[b]	
1010	T1010	1.05:1.95	$LiMnO_2$ (o) + $Li_yMn_{3-y}O_4$ (s) + $LiMn_2O_4$[b]	
1060	T1060	1:2	$LiMnO_2$ (o) + $Li_yMn_{3-y}O_4$ (s) + $LiMn_2O_4$[b]	

[a] Abbreviations: c = cubic, t = tetragonal, o = orthorhombic, s = spinel type, γ = γ-MnO_2 type, β = β-MnO_2. [b] $LiMn_2O_4$ evolves during quenching.

phase diagram is known as a function of temperature. Then the knowledge of the isovalent lines allows extrapolation of the phase diagram to other oxygen partial pressures.

Experimental Section

Extended Time Decomposition. A spinel sample with composition near stoichiometric $LiMn_2O_4$ was prepared by solid-state reaction (sample "stoi790"). Stoichiometric amounts (Mn:Li = 2:1) of Li_2CO_3 (FMC) and EMD (electrolytic manganese dioxide) (Mitsui TAD1, contains 96% MnO_2) were mixed and milled. Pellets (diameter 1 cm, height ≅0.5 cm) were pressed to ensure a homogeneous reaction product. The solid-state reaction was performed for 1 day at 760 °C in air. The powders were milled again, new pellets were pressed, and a second calcination at 790 °C for 16 h followed. The samples were quenched by removing them from the furnace and were ground to powder.

Samples of the powder were filled into alumina crucibles and equilibrated in air at 400, 430, or 550 °C for up to 5 weeks. Occasionally the furnace was opened to remove a small part of the powder for X-ray and TGA analysis.

Investigation of the Phase Diagram. Series of samples with different Li:Mn ratios were prepared in air at different temperatures. Table 2 gives an overview of reaction temperatures and compositions. At 350 and 400 °C, samples were prepared by solid-state reaction of powders of EMD and LiOH in air for a week. The powders were milled, and pellets were pressed, followed by a second calcination for 11 days. To investigate whether equilibrium was reached, the solid-state reaction of newly pressed pellets was continued for 12 more days.

All other sample series were prepared by solid-state reaction of pellets made from the stoichiometric spinel sample "stoi790" with additions of EMD or Li_2CO_3. Solid-state reaction was performed at 550, 800, 880, 890, 920, 940, 950, 1000, 1010, and 1060 °C. Typical reaction times were 5 days (550 °C), 2 days (800 °C), 1 day (880 °C), and 12 h (940 °C). At higher temperatures the Li−Mn system is very reactive, and it is necessary to "freeze" the high-temperature state by quenching. The samples were quenched directly from the furnace into liquid N_2.

The phase composition of the powders was investigated by X-ray diffraction. The X-ray diffraction was performed using a Siemens D500 diffractometer equipped with a copper target X-ray tube and a diffracted beam monochromator. Rietveld profile refinement of the collected data was made using Hill and Howard's version of the Rietveld program.[15]

Oxygen Stoichiometry Measurements. Stoichiometric $LiMn_2O_4$ powder was prepared by solid-state reaction at 750 °C in air. This powder was used to prepare samples of $Li_{1+x}Mn_{2-x}O_4$ ($x = 0$, 0.033, 0.06, 0.07, 0.095, 0.15, and 0.20) by adding measured amounts of lithium salt and making a second solid-state reaction. The samples are the same ones (A1, A2, A3, A4, H3, H4) as investigated in ref 5. These samples were investigated by solid electrolyte coulometry (SEC).

Just before any SEC measurement the powders were annealed at typically 400 °C for 4 h in air or in a gas flow of defined oxygen partial pressure. Then the samples were cooled slowly (−1 °C/min) to room temperature. The gas flow (typically 5 L/h) was prepared by mixing oxygen and argon, or by permeation of oxygen from the air through a silicon rubber hose into the gas flow. A YSZ oxygen sensor controlled the oxygen partial pressure of the gas.

The change of the oxygen stoichiometry was measured by solid electrolyte coulometry of oxygen in the flowing gas. The measurements were performed during a stay of J.M.P. at the Institute for Anorganic Chemistry of the Technical University Dresden, Germany. The SEC apparatus ("Oxylyte", Sensotech GmbH, Magdeburg, Germany) consists of two identical cells, with a reactor in between. Each cell contains a "titration" cell which allows oxygen to be pumped electrochemically into or out of the gas flow and an oxygen sensor which checks the actual oxygen partial pressure of the gas flow after the titration cell. Both sensor and cell are made of platinized tubes of yttria-stabilized zirconia, which is an oxygen ion conducting electrolyte. The first cell prepares and checks the $p(O_2)$ of the gas flow into the reactor, whereas the second cell measures the $p(O_2)$ after the reactor and obtains the oxygen released by the sample by coulometric titration. Further details regarding the device and the titration principle are described in ref 16.

A typical experiment is as follows: a few milligrams of the freshly prepared sample is placed in the quartz tube in the furnace, and the argon gas flow (5 L/h) is switched on. The argon flow was wetted by bubbling at room temperature through water. In the first cell the $p(O_2)$ of the gas flow was fixed to 5×10^{-5} atm by pumping some oxygen into the flow; in the second cell (almost all) oxygen is titrated out of the gas. The $p(O_2)$ after the second cell is fixed to 2×10^{-6} atm. After some time the titration current does not change anymore. A stable "baseline" current is reached. Now the sample is heated (3.5 °C/min) until typically 600 °C. At sufficiently high temperatures (≅300 °C) the equilibration of the sample with the gas phase becomes sufficiently fast. The sample then releases oxygen. The titration current will adjust by an amount corresponding to the amount of oxygen the sample released to hold $p(O_2)$ after the second cell constant. The amount of oxygen released is obtained by the difference between the titration current and baseline current. This is called the "oxygen release current" in this work. The time integral of the oxygen release current gives the change in oxygen stoichiometry of the sample.

Figure 4 shows a typical SEC measurement of the stoichiometric spinel sample. The temperature and oxygen release current are given versus time. The measurement was repeated with a fresh sample, and the two experiments coincide well. At 470 °C, the sample begins to release significant amounts of oxygen. At about 570 °C, the oxygen release becomes small again, but it increases again above 600 °C. This temperature is T_{c1} and is marked by an arrow in Figure 4. The second measurement was interrupted just before T_{c1}, and after cooling in the argon flow (whereby the oxygen stoichiometry is almost fixed), this sample (with maximum oxygen deficiency) was investigated by X-ray analysis, as described later.

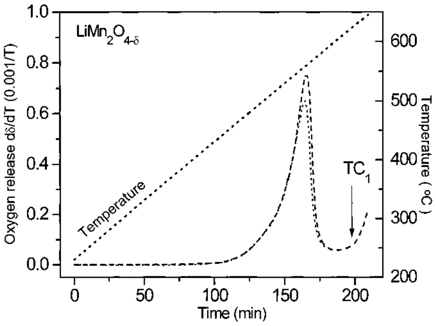

Figure 4. Measurement of the oxygen release of stoichiometric spinel $LiMn_2O_4$ during heating. The integration until T_{c1} gives an oxygen release $\Delta\delta \cong 0.016$.

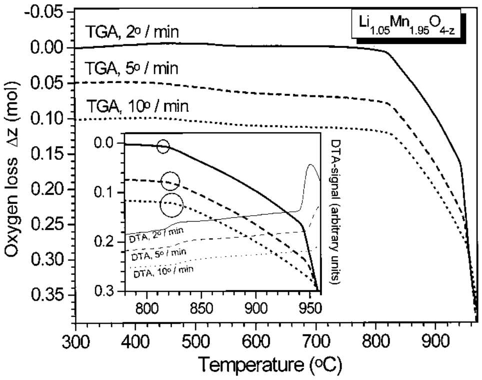

Figure 5. Measurement of T_{c1} of $Li_{1.05}Mn_{1.95}O_4$ in air by TGA using different temperature sweep rates. The various data are offset for clarity. The point of T_{c1} is marked by a circle on each data set.

The disproportionation reaction that begins at T_{c1} is very fast. As a result, the SEC experiments were stopped just after the onset of T_{c1} to avoid saturation of the instrument. Notice the much improved resolution of the SEC (Figure 4) compared with TGA experiments shown in Figure 5. Below T_{c1} a TGA detects almost no oxygen loss. Only the strong oxygen release after T_{c1} is detected in the TGA by the weak change of slope.

The following information can be obtained from the SEC measurement:

The amount of "weakly bound" oxygen is the amount of oxygen that the sample releases during the measurement *before* the decomposition reaction starts at T_{c1}. This amount is obtained by integrating the oxygen release current until the minimum just before T_{c1}. Weakly bound oxygen is probably oxygen in equilibrium with the gas phase, released from the bulk. It is not crystal or adsorbed water (which cannot be detected by SEC).

The onset temperature is the temperature at which the sample begins to release measurable amounts of oxygen. It is a measure of the reduction stability and kinetics and gives information about how easily the "weakly bound" oxygen can be removed from the sample. This temperature cannot be sharply defined.

The disproportionation temperature T_{c1} is the beginning of the increase of the oxygen release current (marked by an arrow in Figure 4) due to disprorportionation reaction. T_{c1} is a function of the lithium stoichiometry and of the oxygen partial pressure.

SEC measurements give exact information about the change of oxygen stoichiometry. They do not give information about the absolute oxygen stoichiometry. In this work, oxygen deficiency is measured relative to the sample which was pretreated in pure oxygen at 400 °C and then slowly cooled to room temperature.

Gao and Dahn suggested the application of TGA to monitor the lithium stoichiometry by measuring T_{c1}.[3] This could be done better using SEC in flowing gas since SEC has a much higher resolution. Furthermore, SEC allows faster measurements than TGA. Figures 5 and 6 show that SEC measurements give identical values for T_{c1} at a variety of sweep rates,

---

(15) Hill, R. J.; Howard, C. J. *J. Appl. Crystallogr.* **1985**, *18*, 173. Wiles, D. B.; Young, R. A. *J. Appl. Crystallogr.* **1981**, *14*, 149.

(16) Teske, K.; Ullmann, H.; Trofimenko, N. *J. Thermal Anal.* **1997**, *49*, 1211.

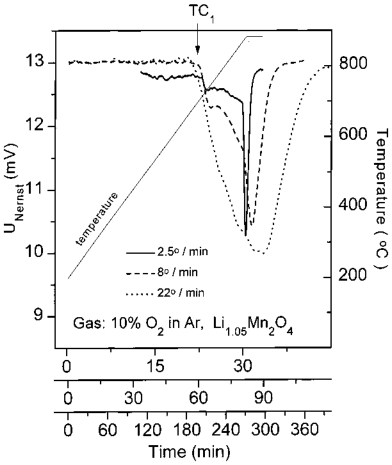

Figure 6. Measurement of T_{c1} of $Li_{1.05}Mn_{1.95}O_4$ by SEC in carrier gas using different temperature sweep rates. The y axis gives the Nernst voltage $U_N = -(RT/4F)\ \ln(p(O_2)/0.21)$ for the gas flow after the sample.

while TGA and DTA measure higher values for T_{c1} when the sweep rates are faster. This is because the latter two techniques measure the bulk changes while SEC is sensitive to the very first oxygen loss.

Results and Discussion

Overview. The construction of the phase diagram in Figure 1 involves a number of steps. The first section, Extended Time Decomposition of Spinel, shows that a lower stability line x_{min} exists. This stability line is probably a function of temperature and $p(O_2)$, $x_{min} = x_{min}(T, p(O_2))$. Spinel $Li_{1+x}Mn_{2-x}O_4$ with $x < x_{min}$ is not stable and decomposes slowly. The next section, Dependence of T_{c1} on Partial Pressure and Lithium Stoichiometry, investigates the upper stability line $x_{max}(T, p(O_2))$. An alternate way to express this line is the critical temperature $T_{c1}(p(O_2), x)$. Spinel $Li_{1+x}Mn_{2-x}O_4$ with $x > x_{max}(T, p(O_2))$ is not stable and decomposes quickly. Thus, spinel exists only between these two lines in a limited stoichiometry range $x_{max} > x > x_{min}$, depending on T and $p(O_2)$. The section Investigation of the Li−Mn Phase Diagram discusses the "overall" phase diagram. It investigates the equilibria of spinel with thermodynamic neighbor phases as well as the structure of spinel phases inside the spinel stability region as a function of Li:Mn ratio. For applications, the stability region of cubic spinel (between 400 and 800 °C) is most interesting. The section Measurements of the Oxygen Stoichiometry by SEC focuses on the oxygen stoichiometry of spinel. It will be shown that the oxygen nonstoichiometry of cubic spinel is negligible. The following section, The Binary Phase Diagram, displays the phase information in a phase diagram of the second kind. A close examination of the phase diagram raises two hypotheses about the exact composition of cubic spinel. The section Structure of Cubic Spinel shows that only cation-mixed spinel $Li_1[Li_xMn_{2-x}]O_4$ is stable between 400 and 880 °C. The possibility that manganese-deficient spinel, $Li_1Mn_{2-x}O_4$, exists above 400 °C will be rejected. In the following section, Cation Deficient Spinel, it will be shown that no proof for the existence of further phases mentioned in the literature (and contradicting our phase diagram) exists. The final section, Applications of the Phase Diagram, discusses applications and consequences of the displayed phase diagram.

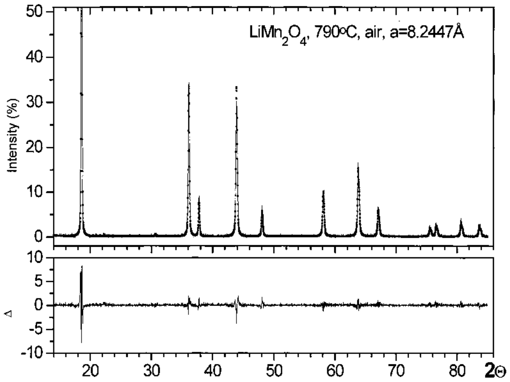

Figure 7. X-ray diffraction pattern and Rietveld refinement of the $LiMn_2O_4$ used for the extended time decomposition experiment.

Extended Time Decomposition of Spinel. Figure 7 shows the X-ray pattern of the stoichiometric spinel after preparation (solid line). The lattice constant (a = 8.248 Å) and Rietveld refinement (Table 3) indicate that the sample is cubic spinel with a composition near $Li_{1.0}Mn_{2.0}O_4$.

Figure 8 shows the diffraction patterns of the sample after it had been subsequently heated at 400 °C for 23 days and at 550 °C for 33 days. Figure 9 shows the change of the cubic lattice constant measured at intervals during the thermal treatment of this spinel sample. Each lattice constant is obtained from a Rietveld refinement. The lattice contracts with exposure time. The lattice constant variation is consistent with an increase of manganese oxidation state. The decomposition of the spinel occurs very slowly, and equilibrium is not reached in these experiments. For comparison, the data of Endres et al.[6] are also plotted. There a more rapid decomposition was observed. This is probably a kinetic effect, which could be caused by different microstructure leading to different diffusion lengths. (Their sample was prepared using $LiOH{\cdot}H_2O$ not Li_2CO_3.) Figure 8 shows that a second phase appears in each of the samples after extended heating. At T = 400 °C this phase can be identified as Mn_5O_8 (JCPDS, ICDD number 20-0718). At 550 °C it is Mn_2O_3 (ICDD number 24-0508).

The mechanism of decomposition seems different at 400 and 550 °C. The lattice constant changes from 8.2477 to 8.2385 Å after 33 days at 550 °C. At 550 °C cation-mixed $Li_{1+x}Mn_{2-x}O_4$ is stable. Using the relation between stoichiometry and lattice constant (Figure 2) yields a final stoichiometry $x \cong 0.06$. Therefore, approximately $0.03Mn_2O_3$ is expected as the second phase. This agrees roughly with the peak intensities in Figure 8. The decomposition mechanism is

$$LiMn_2O_4 + \frac{x}{4(1+x)}O_2 \Rightarrow \frac{1}{1+x}Li_{1+x}Mn_{2-x}O_4 + \frac{3x}{2(1+x)}Mn_2O_3 \quad (8)$$

The situation is different at 400 °C. The lattice constant changes to 8.229 Å. This could indicate a final composition of $Li_{1.09}Mn_{1.91}O_4$. Then $0.09MnO_2$ is expected as the second phase. However, only small peaks of a Mn_5O_8-type phase (ICDD 20-0718) appear. MnO_2

Table 3. Results of the Rietveld Refinements for Cubic Spinels

no.	stoichiometry used in prep	*T* of prep (°C)	*a* (Å)	Li occ on 16d	O pos of 32e	GOF	R_B
stoi790	$LiMn_2O_4$	790	8.245	−0.072	0.263	1.89	3.24
B550	$Li_{1.14}Mn_{1.86}O_4$	550	8.202	0.075	0.263	1.66	2.30
B800	$LiMn_2O_4$	800	8.249	−0.047	0.262	1.70	3.44
B880	$LiMn_2O_4$	880	8.255	−0.005	0.262	1.21	3.52

[a] Fixed parameters: oxygen occupation (32e) equals 4, Li occupation on 8a equals 1, total occupation (Li + Mn) on 16d equals 2. *a* is cubic lattice constant. GOF = goodness of fit. R_B = Bragg *R* factor.

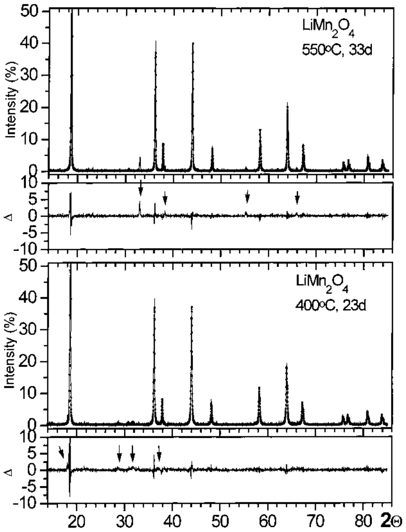

Figure 8. X-ray diffraction pattern of $LiMn_2O_4$ and Rietveld refinement after the extended time thermal treatment. Upper plot: 33 days at 550 °C; second phase Mn_2O_3. Lower plot: 23 days at 400 °C; second phase Mn_5O_8.

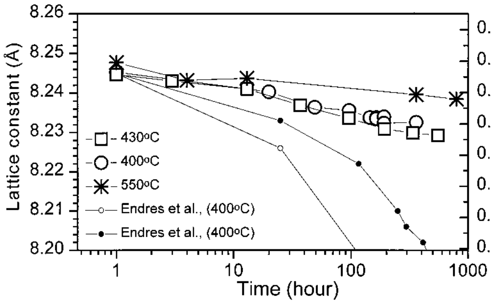

Figure 9. Change of lattice constant of $LiMn_2O_4$ during the extended time thermal treatment. Data from ref 6 are also shown.

and Mn_5O_8 are phases which can have disordered structures and hence X-ray spectra with broad peaks, which could appear weak as observed.

The decrease of the lattice parameter at 400 °C, however, could have an alternative explanation. Certainly, the decrease is caused by the increase of the mean Mn oxidation state since the ionic radius of Mn^{4+} is smaller than the ionic radius of Mn^{3+}. The Mn oxidation state can be changed by oxygen nonstoichiometry. Possibly the decomposition occurs through an intermediate oxygen-rich spinel such as $LiMn_2O_4 \Rightarrow LiMn_2O_{4+y}$. The intermediate phase then decomposes very slowly to the final stable cation-mixed spinel $Li_{1+x}Mn_{2-x}O_4$ (or alternately to manganese-deficient spinel, $LiMn_{2-x}O_4$, coexisting with manganese oxide). The possible existence of an oxygen-rich spinel phase, $Li_2Mn_4O_9$ (which is metastable above 400 °C), is proposed in refs 17 and 18. The decomposition in Figures 8 and 9 is reversible. A sample that decomposed at 400 °C for 15 days was heated to 780 °C for 10 h. The initial lattice constant of the freshly prepared stoichiometric spinel was recovered.

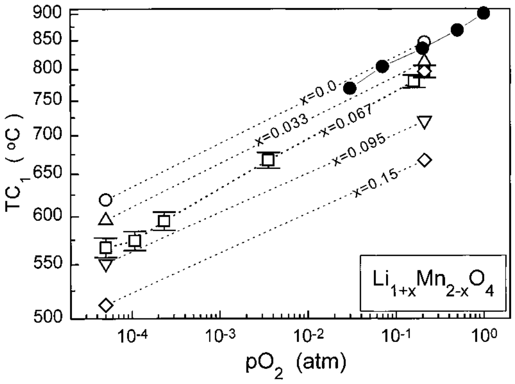

Figure 10. Decomposition temperature T_{c1} of $Li_{1+x}Mn_{2-x}O_4$ as a function of $p(O_2)$ and composition *x*. Filled circles: Results for $LiMn_2O_4$ from Yamada et al.[10]

Dependence of T_{c1} on Partial Pressure and Lithium Stoichiometry. T_{c1} is the upper stability line of spinel. Heating spinel in equilibrium with the $p(O_2)$ of the gas phase leads to a large oxygen release at T_{c1}. T_{c1} as a function of composition, *x*, in $Li_{1+x}Mn_{2-x}O_2$ and $p(O_2)$ was measured by SEC as shown in Figure 4. In high partial pressures (air, oxygen) TGA results were used. Figure 10 shows the dependence of T_{c1} on *x* as a function of partial pressure. The results of Yamada et al.[10] are also displayed. T_{c1} decreases with decreasing oxygen partial pressure. Since T_{c1} for a given *x* is the upper stability limit of the spinel phase with this stoichiometry, T_{c1} versus $p(O_2)$ is an isostoichiometric or isovalent line. Its slope allows the calculation of the partial reaction enthalpy of the oxygen release.

$$Li_{1+x}Mn_{2-x}O_4 \leftrightarrow (1-x)LiMn_2O_4 + xLi_2MnO_3 + (x/2)O_2, \quad \Delta H/x = 56\ \text{kJ/mol} \quad (9)$$

Investigation of the Li−Mn Phase Diagram. Spinel is stable in the region between the lower and upper stability lines. The position of the upper stability line T_{c1} is exactly known. This section investigates samples with varying Li:Mn ratios prepared at different temperatures in air. The goal is to find the position of the lower stability line and to study the structure of the spinel. Figures 11−15 show the X-ray diffraction patterns of samples with different Li:Mn ratios prepared at *T* = 400, 550, 800, 880, and 940 °C. These figures will be explained sequentially below.

(1) 400 °C, Figure 11. Sample A with Li:Mn = 4:5 is almost single-phase cubic spinel $Li_4Mn_5O_{12}$. The weak

---

(17) Thackeray, M. M.; Rossouw, M. H. *J. Solid State Chem.* **1994**, *113*, 441.

(18) de Kock, A.; Rossouw, M. H.; Picciotto, L. A.; Thackeray, M. M. *Mater. Res. Bull.* **1990**, *25*, 665.

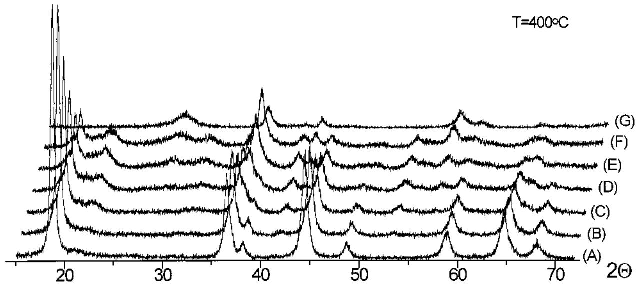

Figure 11. X-ray diffraction patterns of a series with varying Li:Mn ratios prepared at 400 °C in air. Li:Mn ratios: (A) 4:5, (B) 3.5:5.5, (C) 1:2, (D) 2.5:6.5, (E) 2:7, (F) 1.5:7.5, (G) 0:1.

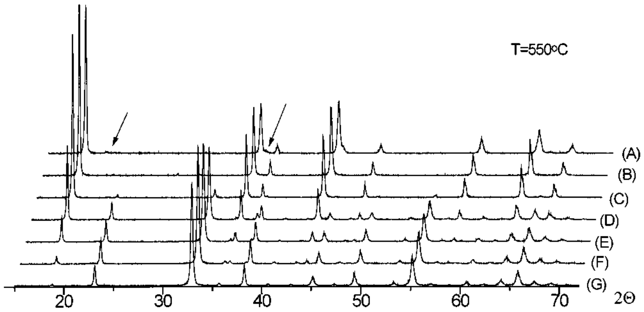

Figure 12. X-ray diffraction patterns of a series with varying Li:Mn ratios prepared at 550 °C in air. Li:Mn ratios: (A) 1.5:2, (B) 1.23:2, (C) 1:2, (D) 0.5:2, (E) 0.2:2, (F) 0.1:2, (G) 0:2. Arrows: Li_2MnO_3.

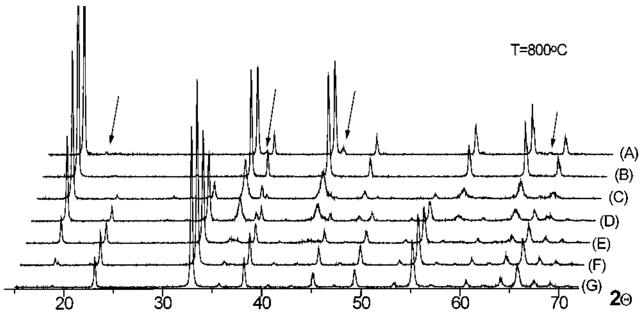

Figure 13. X-ray diffraction patterns of a series with varying Li:Mn ratios prepared at 800 °C in air. Li:Mn ratios: (A) 1.22:2, (B) 1:2, (C) 0.8:2, (D) 0.5:2, (E) 0.2:2, (F) 0.1:2, (G) 0:2. Arrows: Li_2MnO_3.

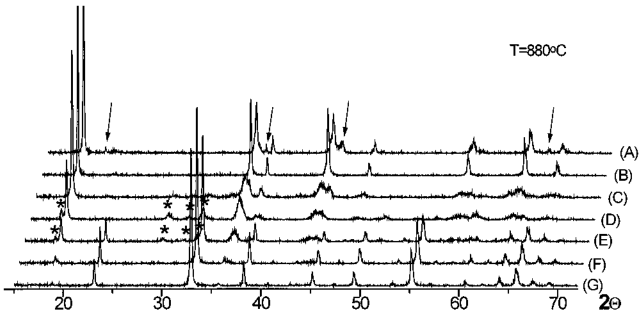

Figure 14. X-ray diffraction patterns of a series with varying Li:Mn ratios prepared at 880 °C in air. Li:Mn ratios: (A) 1.25:2, (B) 1:2, (C) 0.8:2, (D) 0.5:2, (E) 0.2:2, (F) 0.1:2, (G) 0:2. Arrows: Li_2MnO_3. Asterisks: Lithiated Hausmanite.

broad peak near 21.5° could be due to traces of lithiated γ-MnO_2. Figure 16 shows the Rietveld refinement that is consistent with $Li_4Mn_5O_{12}$. In the refinement, the lithium occupation of the 8a sites was fixed ($n = 1$), and a replacement of Mn on 16d sites by Li was allowed. The sum of Li and Mn occupations was fixed to 3. The occupation of oxygen at 32e was fixed to 4, and an overall isotropic temperature factor was used. Sample B with Li:Mn = 3.5:5.5 is a two-phase material. This can be seen by the appearance of the main peak of the γ-MnO_2-related phase at $2\theta = 41.2°$ (between the spinel 222 and 004 peak). Sample C, Li:Mn = 1:2, is spinel coexisting with a γ-MnO_2-related phase. The coexistence shows that apparently $Li_2Mn_4O_9$ is not stable at 400 °C.

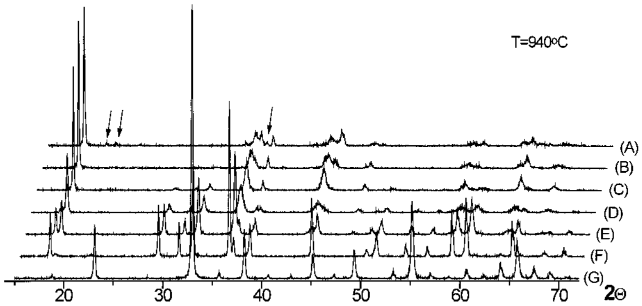

Figure 15. X-ray diffraction patterns of a series with varying Li:Mn ratios prepared at 940 °C in air. Li:Mn ratios: (A) 1.25:2, (B) 1:2, (C) 0.8:2, (D) 0.5:2, (E) 0.2:2, (F) 0.1:2, (G) 0:2. Arrows: Li_2MnO_3.

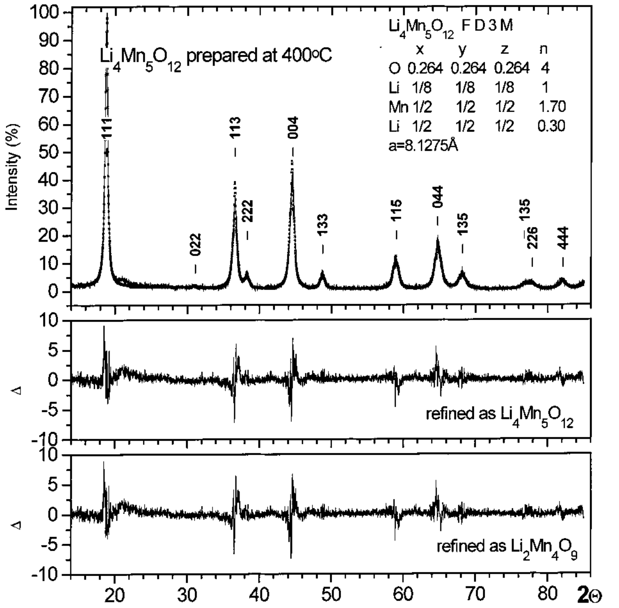

Figure 16. X-ray diffraction pattern and Rietveld refinement for $Li_4Mn_5O_{12}$ prepared at 400 °C. Upper plot: Measured and calculated spectrum. Middle plot: Difference between the measured spectrum and the spectrum calculated for $Li_4Mn_5O_{12}$. Lower plot: Difference between the measured spectrum and the spectrum calculated for $Li_2Mn_4O_9$, showing the difficulty in distinguishing $Li_2Mn_4O_9$ and $Li_4Mn_5O_{12}$.

Samples D−F with compositions Li:Mn = 2.5:6.5, 2:7, and 1:5 are all three-phase mixtures of spinel, a γ-MnO_2-related phase (peaks at 22°, 32°, 37°, and 53° 2θ) and β-MnO_2 (peaks at 28°, 37°, and 57° 2θ). This is shown for sample F in Figure 17. The lower plot shows the spectrum of sample F after subtracting the spinel spectrum. The upper plot shows β-MnO_2 (sample G) whereas the middle plot shows sample A350 that is predominantly γ-$Li_{0.33}MnO_2$ prepared at lower temperature. With decreasing Li:Mn ratio the spinel phase vanishes and the γ- and β-MnO_2 phases evolve. The ratio of the γ- to the β-phase decreases.

The coexistence of three phases is possible (as discussed before in the theoretical section) since the

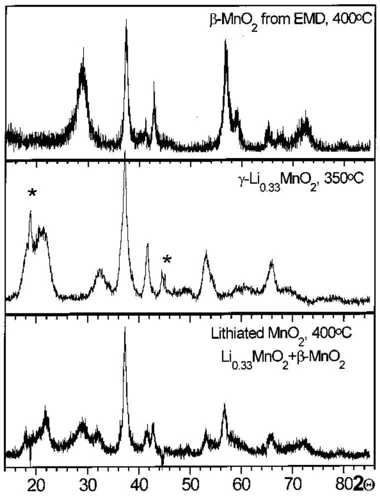

Figure 17. X-ray diffraction pattern of MnO_2 and lithiated MnO_2 prepared in air. Upper plot: Pure MnO_2 (β-MnO_2) (400 °C). Middle plot: $Li_{0.33}MnO_2$ (γ-MnO_2 type) (350 °C). Asterisks: $Li_4Mn_5O_{12}$ impurity. Lower plot: Lithiated MnO_2 (mixture of γ-MnO_2 + β-MnO_2 type) (400 °C).

γ-phase is at its upper stability temperature. The abrupt change from F to G indicates that the γ-MnO_2 phase contains lithium. γ-MnO_2 has a channel structure with predominantly 2 × 1 tunnels.[19] Stabilization by Li cations located in the channels prevents the collapse of the structure. Therefore, sample G, without lithium, is β-MnO_2.

A careful analysis of the X-ray data of C−G gives the composition of the phases as $Li_{1.1}Mn_{1.9}O_{4+\delta}$ (spinel), $Li_{0.3}MnO_2$ (γ-MnO_2 phase), and MnO_2 (β-MnO_2). The lattice constant of the spinel phase ($a \cong 8.13$ Å) is similar to that of $Li_4Mn_5O_{12}$ (sample A, $a = 8.127$ Å) and near $a = 8.162$ Å for $Li_2Mn_4O_9$.[17] It differs significantly from $a \cong 8.22$ Å for $Li_{1.1}Mn_{1.9}O_4$ (lattice constant a obtained from Figure 2). This indicates that the spinel at 400 °C is a member of the tie-line $Li_2Mn_4O_9$−$Li_4Mn_5O_{12}$ and has the stoichiometry $Li_{1.1}Mn_{1.9}O_{4+\delta}$ ($\delta = 0.35$). This stoichiometry is very near that of the manganese-deficient spinel $LiMn_{1.75}O_4$.

To show that the coexistence of three phases is caused by the vicinity to the decomposition temperature of γ-Li_xMnO_2 (which above 400 °C decomposes to β-MnO_2 and spinel), a sample (A350) was prepared at lower temperatures. LiOH and EMD with Li:Mn = 0.37 reacted at 350 °C in air. The equilibrium stoichiometry of γ-Li_xMnO_2 at 350 °C is known to be near $x = 0.33$.[20] Therefore, in equilibrium, γ-Li_xMnO_2 (with $x \cong 0.33$) should coexist with traces of spinel. This is confirmed in the middle plot of Figure 17.

The solid-state reaction of all samples was continued for 12 more days. The X-ray spectra were reproduced and did not show clear changes so that a state very near equilibrium was guaranteed.

Conclusion. Below 400 °C spinel has a composition on the tie-line $Li_2Mn_4O_9$−$Li_4Mn_5O_{12}$. $LiMn_{1.75}O_4$ coexists with lithiated γ-type MnO_2. $Li_4Mn_5O_{12}$ coexists with Li_2MnO_3. It is believed that $Li_2Mn_4O_9$ is not thermodynamically stable.

(2) 550 °C, Figure 12. Sample A, Li:Mn = 1.5:2 ($a = 8.170$ Å), is spinel coexisting with a small amount of Li_2MnO_3. Sample B (Li:Mn = 1.23:2) is single-phase cubic spinel $Li_{1.14}Mn_{1.86}O_4$ with lattice constant $a = 8.202$ Å.

Table 3 shows the results of the Rietveld refinement. The importance of the cationic stoichiometries obtained from the refinement should not be overestimated. A better measure for the lithium stoichiometry is the lattice constant. The diffraction peaks are narrower than those in Figure 11, showing that the samples are more crystalline compared to spinel at 400 °C. Increasing the Mn content leads to a two-phase equilibrium of cubic spinel with Mn_2O_3 (ICDD number 41-1442). Sample C, Li:Mn = 1:2, is cubic spinel ($a = 8.232$ Å) with a small amount of Mn_2O_3. Sample F with Li:Mn = 0.22:2 still contains spinel, indicating that no lithium is dissolved in Mn_2O_3. Sample G with Li:Mn = 0:1 is pure Mn_2O_3.

Spinel coexisting with Li_2MnO_3 (sample A) will exhibit the highest lithium stoichiometry possible at 550 °C whereas spinel coexisting with Mn_2O_3 (sample C) will have the lowest lithium stoichiometry. The cationic stoichiometry range, which is allowed in equilibrium, is between these values. Unfortunately, the lower limit of this range cannot be obtained from the given X-ray data. The samples, which contain spinel coexisting with Mn_2O_3, have not necessarily reached equilibrium. The equilibration requires the decomposition of the stoichiometric spinel to lithium-rich spinel and Mn_2O_3. This needs months as the extended time decomposition experiment proved.

To speed up the equilibration, a further sample with Li:Mn = 1:2 (acet550) was prepared from a lithium nitrate/manganese acetate solution. The solution was dried (60 °C) and calcined at 250 °C. The solid-state reaction was made at 550 °C. The better mixing of the cations on an atomic scale as well as the oxidizing properties of the nitrate causes a faster equilibration. X-ray investigation reconfirmed the coexistence of cubic spinel and Mn_2O_3. The lattice constant of spinel was 8.231 Å after 2 + 1 days of reaction and 8.229 Å after 2 + 7 days. This confirms that the minimum x is larger than 0.09 in $Li_{1+x}Mn_{2-x}O_4$.

Conclusion. Cubic spinel $Li_{1+x}Mn_{2-x}O_4$ ($0.09 < x \leq 0.22$) is stable. Spinel coexists with Li_2MnO_3 or with Mn_2O_3.

(3) 800 °C, Figure 13. Sample B with Li:Mn = 1:2 is single-phase spinel with lattice constant $a = 8.249$ Å. Table 3 gives the results of the Rietveld refinement. Sample A with Li:Mn = 1.22:1 is spinel coexisting with Li_2MnO_3. The lattice constant is $a = 8.236$ Å, indicating that the highest lithium stoichiometry at 800 °C is about $x = 0.06$. Samples C−F are spinels (lithium stoichiometry at its lower limit) coexisting with Mn_2O_3. The lattice constant $a = 8.249$ Å gives the lower lithium stoichiometry limit as $x = 0$. Sample G is pure Mn_2O_3. No significant amount of lithium is soluble in Mn_2O_3.

Conclusion. The spinel phase is stable from about $x = 0$ to $x = 0.06$. Cubic spinel $Li_{1.06}Mn_{1.94}O_4$ coexists with Li_2MnO_3. Mn_2O_3 coexists with stoichiometric spinel.

(4) 880 °C, Figure 14. Sample A with Li:Mn = 1.25:2 is spinel ($a = 8.258$ Å) coexisting with Li_2MnO_3. Sample B with Li:Mn = 1:2 is a single-phase cubic spinel with

---

(19) Chabre, Y.; Pannetier, J. *Prog. Solid State Chem.* **1995**, *23*, 1−130.

(20) Dahn, J. R.; Way, B. M. U.S. Patent US4959282, 1990.

lattice constant $a = 8.255$ Å. The results of the Rietveld refinement are given in Table 3. Sample G with Li:Mn = 0:2 is pure Mn_2O_3. Adding lithium to manganese oxide (sample F with a ratio of Li:Mn = 0.1:2, and sample E, with Li:Mn = 0.2:2) leads to two-phase equilibria of Mn_2O_3 with a tetragonal spinel or/and a Mn_3O_4-type phase which contains lithium (lithiated Hausmanite). Sample E shows an interesting phase composition. It is a three-phase equilibrium of spinel, lithiated Hausmanite (marked by asterisks in Figure 14), and Mn_2O_3. The equilibrium of three phases by the Gibbs phase rule is allowed as discussed in the theoretical section if a further freedom is fixed (similar to the triple point of water). This is the case if the lithiated Hausmanite is at its lower decomposition temperature. The temperature in a furnace is not constant but fluctuates. Sometimes it is above the decomposition temperature, and Hausmanite is formed. At other times it is below, and spinel will be formed instead. The result is the coexistence of the three phases.

Further lithium increase (sample D, Li:Mn = 0.5:2) leads to a phase equilibrium of the lithiated Hausmanite with spinel. This spinel is lithium deficient and has a composition of approximately $[Li_{0.9}Mn_{0.1}]Mn_2O_4$. The crystal structure of the lithium-deficient spinel shows a weak tetragonal distortion, space group $I4_1/amd$. This phase differs from the tetragonal spinels observed by Tarascon (ref 4) which exhibit a large tetragonal distortion. It is also different from the tetragonal spinel suggested by Thackeray (ref 11) which is lithiated Hausmanite. Sample C with Li:Mn = 0.8:2 is tetragonal spinel with additional traces of the lithiated Hausmanite. The spinel phase exhibits a complicated diffraction pattern. The tetragonal distortion is small ($\sqrt{2}a/c \approx 1.014$). The upper panel in Figure 18 shows the Rietveld refinement of this tetragonal spinel phase. In the refinement the oxygen occupation on 32a was fixed at 4, the manganese occupation on 16d was free, and Mn was allowed to replace Li on 8a sites.

Conclusion. The lower stability temperature of lithiated Hausmanite with a composition of about $Li_{0.2}Mn_{2.8}O_4$ is 880 °C. A weakly distorted tetragonal spinel $[Li_{0.9}Mn_{0.1}]Mn_2O_4$ coexists with Mn_2O_3 or lithiated Hausmanite $Li_{0.2}Mn_{2.8}O_4$. Cubic spinel $LiMn_2O_4$ ($a = 8.255$ Å) coexists with Li_2MnO_3.

(5) 940 °C, Figure 15. Samples A (Li:Mn = 1.25:2), B (Li:Mn = 1:2), and C (Li:Mn = 0.8:2) are tetragonal spinels. A is in equilibrium with Li_2MnO_3, and C is in equilibrium with Mn_3O_4. The composition of the spinel phase is approximately $[Li_{0.95}Mn_{0.05}]Mn_2O_4$. The Rietveld refinement of the single-phase sample B is shown in Figure 18, lower plot. Sample G (from pure EMD) is Mn_2O_3. Addition of lithium to the manganese oxide leads to lithiated Hausmanite. Sample F (Li:Mn = 0.1:2) is single-phase lithiated Hausmanite, with tiny additions of tetragonal $Li_{1-x}Mn_{2+x}O_4$ spinel. Further addition of lithium leads to coexistence of the lithiated Hausmanite with tetragonal spinel.

Thackeray suggested that, above 915 °C, Li_2MnO_3 and $LiMn_2O_4$ decompose to yield $LiMnO_2$.[11] Our data show that both Li_2MnO_3 and a manganese-rich spinel $[Li_{0.9}Mn_{0.1}]Mn_2O_4$ are still stable at 940 °C.

(6) 1000 and 1060 °C. The X-ray diffraction patterns show three phases. Orthorhombic $LiMnO_2$ (rock salt structure) coexists with lithiated Hausmanite. Additional peaks due to Li−Mn spinel are present. The latter phase is probably caused by kinetics and develops during quenching ($LiMnO_2 + (1/3)Mn_3O_4 + (1/3)O_2 \Rightarrow LiMn_2O_4$). To increase the quenching rate, a further pellet was quenched in water. The intensity of the Li−Mn spinel phase in the spectrum was reduced by about 60%. We were not able to quench quickly enough to suppress the back reaction to the Li−Mn spinel phase. The high-temperature X-ray data of ref 11 show a two-phase equilibrium of spinel with $LiMnO_2$ above 1000 °C. We want to emphasize that this spinel is lithiated Hausmanite $[Mn_{1-x}Li_x]MnO_4$ instead of the proposed $[Li_{1-x}Mn_x]Mn_2O_4$. Both phases are members of the "spinel" tie-line Mn_3O_4−$LiMn_2O_4$. However, they are separated and do not make a solid solution.

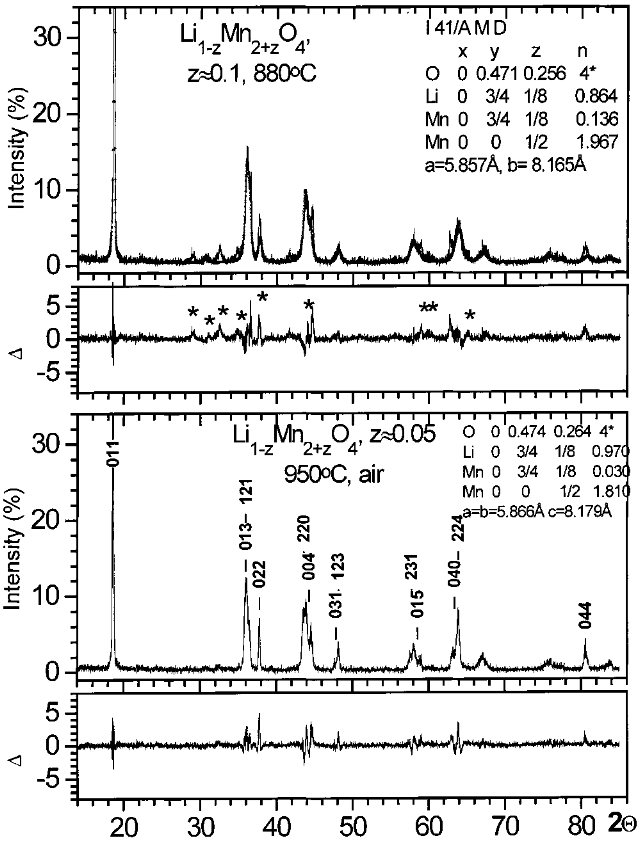

Figure 18. X-ray diffraction pattern and Rietveld refinement of weak distorted tetragonal spinel. Upper plot: $[Li_{0.9}Mn_{0.1}]Mn_2O_4$ prepared at 880 °C. The asterisks mark the peaks of the coexisting lithiated Hausmanite impurity. Lower plot: $[Li_{0.95}Mn_{0.05}]Mn_2O_4$ prepared at 940 °C.

(7) Further Results at High Temperatures. Since Tarascon et al. (ref 4) observed a lithium manganese spinel phase with a large tetragonal distortion at 905 °C, we equilibrated $Li_{1.05}Mn_{1.95}O_4$ at $T = 890$, 920, 950, 980, and 1100 °C followed by quenching in water. Indeed, at 920 °C the desired tetragonal phase (with composition approximately $[Li_{0.95}Mn_{0.05}]Mn_2O_4$) coexists with Li_2MnO_3. The unit cell is stretched along the tetragonal c axis ($\sqrt{2}a/c = 0.94$). The Rietveld refinement does not support the assumption of oxygen deficiency, Figure 19, upper plot. Surprisingly, another tetragonal phase with an "inverse" distortion exists. At 890 °C a spinel phase with similar composition but compressed c axis coexists with Li_2MnO_3. Here the degree of distortion depends on thermal history before

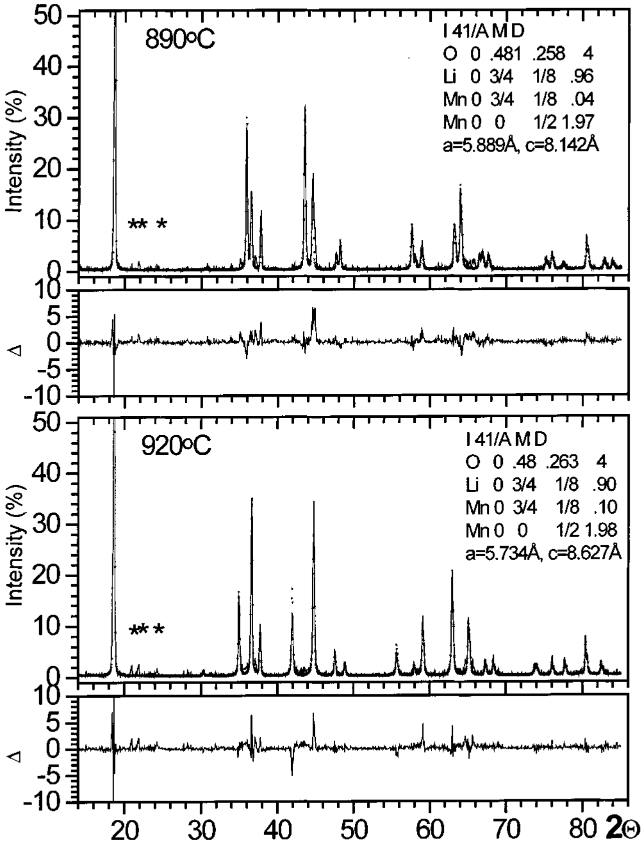

Figure 19. X-ray diffraction pattern and Rietveld refinement of tetragonal spinel. Upper plot: $[Li_{0.95}Mn_{0.05}]Mn_2O_4$ prepared at 920 °C. Lower plot: $[Li_{0.95}Mn_{0.05}]Mn_2O_4$ prepared at 890 °C. The asterisks mark the peaks of the coexisting Li_2MnO_3 impurity.

the equilibration. We obtained $\sqrt{2}a/c = 1.015$ after cooling to 890 °C and 1.023 after heating to the same temperature. The Rietveld refinement of the phase equilibrated after cooling is shown in the lower plot of Figure 19.

At higher temperatures (980 °C) a weakly distorted spinel with larger lithium deficiency coexists with $LiMnO_2$ (orthorhombic), and at 1010 °C Mn_3O_4 begins to be stable instead of Li−Mn spinel. A detailed discussion of the high-temperature region would exceed the scope of this work.

Conclusion. At temperatures above 1000 °C lithiated Hausmanite coexists with orthorhombic $LiMnO_2$. The Li−Mn spinel phase is not stable anymore. However, the back reaction to spinel during quenching is very fast. In the region between 880 and 980 °C a variety of tetragonal spinel phases are stable. The unit cell is elongated (920 °C) or compressed (890 °C). The tetragonal distortion becomes smaller at the lower (880 °C) and higher (980 °C) limits as well as for manganese-rich phases (coexisting with Mn_3O_4). No clear hint for oxygen deficiency was observed.

Measurements of the Oxygen Stoichiometry by SEC. Stoichiometric spinel was thermally pretreated at 400 °C in gases with different oxygen partial pressures. Just after the thermal treatment the samples were put into the SEC reactor and the oxygen release into the argon flow was measured. A typical measurement is shown in Figure 4. The sample was pretreated in air at 400 °C. The integrated oxygen release until T_{c1} is reached would give δ in a spinel $LiMn_2O_{4-\delta}$ with oxygen nonstoichiometry. The results of a series of such measurements are shown in the left plot of Figure 20. The *x* axis gives the partial pressure of the gas used during the thermal treatment. $\delta = 0$ is defined as the oxygen stoichiometry which the sample had after a thermal treatment in oxygen for 7 h as described earlier.

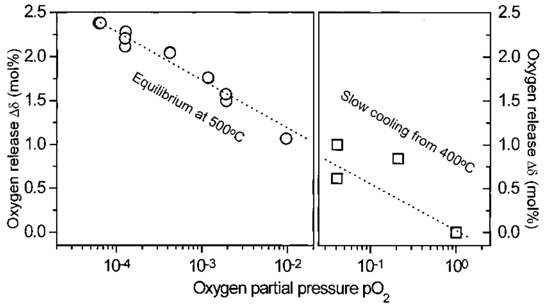

Figure 20. Oxygen stoichiometry change of spinel $LiMn_2O_4$ to $LiMn_2O_{4-\delta}$. Left plot: Stepwise change of partial pressure. Right plot: Heating in gas flow with given $p(O_2)$.

The right-hand part of Figure 20 gives the oxygen release of stoichiometric spinel that is in equilibrium with a gas having $p(O_2) = 0.01$ at 500 °C after stepwise changing the partial pressure of the flowing gas to lower and lower $p(O_2)$ (2×10^{-3}, 1×10^{-3}, 3×10^{-4}, 1×10^{-4}, 5×10^{-5}). This measurement is less exact, but it allows stoichiometry changes to be measured over a wider range of partial pressures.

On first glance the results indicate that spinel $LiMn_2O_{4-\delta}$ is a material with an oxygen stoichiometric range ($\delta = 0$ to $\delta = 0.025$) which depends smoothly on the partial pressure of the gas. The deficiency increases with decreasing partial pressure. A sample in equilibrium with argon with a $p(O_2)$ of 2×10^{-5} atm at 500 °C, for example, has a deficiency of $\delta \cong 0.024$ compared to a sample pretreated in oxygen.

However, the results must be discussed further. The extended time decomposition experiment proves that stoichiometric spinel is not stable at temperatures near 400−500 °C. Therefore, a partial decomposition of stoichiometric spinel to lithium-rich spinel and manganese oxide will have occurred during the thermal treatment. Consequently, the apparent measured oxygen stoichiometry range must not only be caused by the change of the oxygen stoichiometry of the spinel phase. It is also caused by an oxygen release due to the decomposition of the additional manganese oxide. For example, at 400 °C in oxygen MnO_2 is stable.[21] During the SEC measurement it will decompose to $Mn_2O_3 = 2MnO_2 - (1/2)O_2$. So the results of Figure 20 do not give the oxygen stoichiometric range of spinel. Rather, it gives an upper limit for the oxygen stoichiometry range.

Figure 4 shows two measurements of the oxygen release of two identical samples of stoichiometric spinel (the samples were pretreated in air at 400 °C). The second measurement was switched off just before T_{c1} was reached and the sample cooled in the argon flow. During cooling these samples generally want to uptake oxygen. However, the oxygen partial pressure of the argon flow is sufficiently small to suppress significant

---

(21) Gurvich, L. V.; Iorish, V. S.; D. V. *Ivtan Thermo, Database on thermodynamic properties of individual substances,* version 1.01; Russian Academy of Science, Begell House, Inc.: New York, 1993.

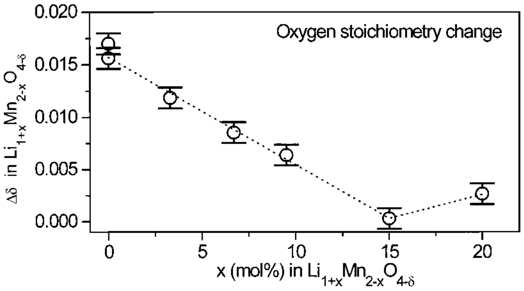

Figure 21. Amount of weakly bound oxygen in $Li_{1+x}Mn_{2-x}O_4$ as a function of lithium stoichiometry x.

changes of the oxygen stoichiometry. The sample was X-rayed after cooling. The lattice constant changed from a = 8.239 Å (fresh sample after thermal treatment in air at 400 °C) to 8.256 Å after cooling in argon. This increase of the lattice constant would be typical for the introduction of oxygen vacancies. The lacking oxygen leads to an increased cationic repulsion and, hence, to a lattice expansion. However, the lattice constant change could also be caused by the back reaction to stoichiometric spinel. During heating in argon the partially decomposed spinel could react with manganese oxide $Li_{1+x}Mn_{2-x}O_4 + 3xMnO_2 \Rightarrow (1 + x)LiMn_2O_4 + (x/2)O_2$.

The amount of "weakly bound oxygen" in a series of samples with different lithium stoichiometries was measured. The samples were pretreated in air as described earlier. Figure 21 shows this amount, given by the release of oxygen before T_{c1}. The release of oxygen decreases with increasing lithium stoichiometry. The decrease can have two causes. First the oxygen stoichiometric range decreases. Second the driving force for the low-temperature decomposition is smaller for lithium-rich spinels. Therefore, during the thermal treatment in air smaller amounts of spinel have decomposed to manganese oxide or to oxygen-rich spinel.

The amount of weakly bound oxygen correlates with the capacity fading of spinel. It is largest for stoichiometric spinel and becomes minimal for lithium-rich spinel $Li_{1+x}Mn_{2-x}O_4$ with $x \cong 0.15$. Measuring the amount of weakly bound oxygen in a large series of spinel samples where corresponding capacity retention results are known could help to understand the capacity fading.

Conclusion. Stoichiometric spinel could have an oxygen stoichiometric range. The range does not exceed $\delta \approx 0.025$ in $Li_{1+x}Mn_{2-x}O_{4-\delta}$. Probably it is much smaller. The oxygen nonstoichiometric range of cation-mixed spinel $Li_{1+x}Mn_{2-x}O_4$ is negligible.

The Binary Phase Diagram. The obtained results can be displayed in a phase diagram of the second kind. Figure 1 shows the phase diagram based on the experiments reported above. This phase diagram should be used to check measurements and interpretations critically. Often, for example, the properties of spinel with a fixed composition are investigated as a function of temperature. This is only meaningful inside the stability region shown in the phase diagram.

The phase diagram shows principally different stability regions for Li−Mn spinel. Between 400 and 880 °C spinel is stable as cation-mixed spinel $Li_{1+x}Mn_{2-x}O_4$. This phase is stable between an upper stability line T_{c1} and a lower stability line, leading to the proposed stability region in Figure 1. The stability of cation-mixed spinel can be explained by the lack of cationic and anionic vacancies. All 8a, 16d, and 32e sites are filled. With increasing temperature the mean Mn oxidation state, ν, decreases. This is enabled by a decrease of x from $x = 1/3$, $\nu = 4$, at 400 °C to $x = 0$, $\nu = 3.5$, at 880 °C.

Above ≅880 °C the average manganese oxidation state is lowered by replacing lithium by manganese, leading to tetragonal spinel $[Li_{1-x}Mn_x]MnO_4$ with $\nu < 3.5$.

Below 400 °C the manganese oxidation state is fixed at its maximum $\nu = 4.0$, leading to spinels on the tie-line $Li_2Mn_4O_9$−$Li_4Mn_5O_{12}$. These low-temperature spinels can hardly be distinguished by X-ray diffraction since their patterns are very similar. However, the analysis of the data in Figure 11 indicated that only the cation-mixed spinel $Li_4Mn_5O_{12}$ and manganese-deficient spinel $LiMn_{1.75}O_4$ are stable on this tie-line.

Reexamining the data shows that an alternative phase diagram for the stability region of spinel between 400 and 880 °C could be possible. This alternative phase diagram (which will be rejected later) is based on the concept of manganese-deficient spinel. It will be explained in the following.

Doubtless, the upper stability line of spinel is given by $Li_{1+x}Mn_{2-x}O_4$, which is the tie-line between $LiMn_2O_4$ (at $T \cong 800$ °C, $\nu = 3.5$) and $Li_4Mn_5O_{12}$ (at $T = 400$ °C, $\nu = 4$). However, the lower stability line must not necessarily be cation-mixed spinel $Li_{1+x'}Mn_{2-x'}O_4$ with $x' < x$. Alternatively it could be manganese-deficient spinel $Li_1Mn_{2-x}O_4$ as a member of the tie-line $LiMn_{1.75}O_4$ (at $T \cong 400$ °C, $\nu = 4$) and $LiMn_2O_4$ ($T \cong 880$ °C, $\nu = 3.5$). This hypothesis is supported by the fact that points at 880, 800, 700, and 550 °C on the lower stability line in Figure 1 and the point at 400 °C for $LiMn_{1.75}O_4$ fit nicely to a line.

Which of the two possible diagrams is correct can be checked by measuring the lattice constant as a function of the Li:Mn ratio. The lattice constant is a function of composition. If the presented phase diagram of Figure 1 is true, then all spinels with similar Li:Mn ratios have the same composition since oxygen or cationic vacancies are rejected. Two spinels with the same Li:Mn ratio, prepared at different temperatures, will therefore have the same lattice constant. If this is not the case, then the alternative phase diagram (the lower stability line is manganese-deficient spinel $LiMn_{2-x}O_4$) is correct. Then spinel near the lower stability line exhibits manganese vacancies. The number of vacancies decreases with increasing preparation temperature to enable the decrease of the mean Mn oxidation state. Therefore, two spinels with the same Li:Mn ratio prepared at different temperatures will have different stoichiometries and different mean manganese oxidation states. Hence, the lattice constant will be a function of preparation temperature for a fixed Li:Mn ratio.

Structure of Cubic Spinel. To check which of the two hypotheses is correct, a further series of spinels was prepared at 800, 700, 550, and 400 °C. At each temperature one sample with Li:Mn ratio 1:2 and further samples with Li:Mn ratios inside the stability region were prepared. Knowledge of the exact Li−Mn stoichi-

Table 4. Li:Mn Ratios and Lattice Constants of Spinel Samples Prepared To Check the "Cation-Mixed" against the "Manganese-Deficient" Hypothesis

T (°C)	Li:Mn	phase composition	*a* (Å)
550	1:2	spinel + Mn_2O_3	8.2225
	1:1.82	spinel	8.2176
	1:1.655	spinel	8.1953
	1:1.485	spinel	8.1673
700	1:2	spinel	8.2427
	1:1.907	spinel	8.2314
	1:1.813	spinel	8.2193
	1:1.72	spinel	8.2074
800	1:2	spinel	8.2400
	1:1.958	spinel	8.2342
	1:1.875	spinel	8.2333
880	1:2	cubic + tetragonal spinel	8.2507 (cubic)

[a] The data are also displayed in Figure 2.

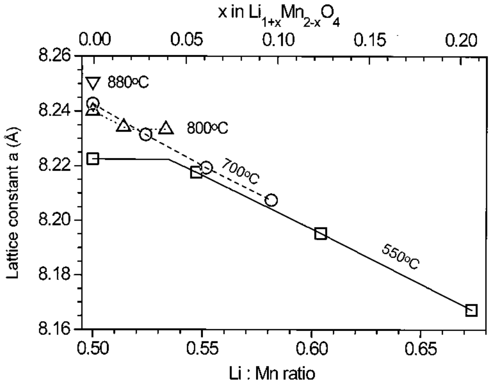

Figure 22. Lattice constant of cubic spinel as a function of lithium stoichiometry.

ometry is essential. Therefore, Mn_2O_3 instead of EMD and Li_2CO_3 ($LiCO_3$ and Mn_2O_3 are nonhygroscopic and stoichiometric) were used as reactants. Large amounts of powder (≅200 g) were carefully mixed and ground. To minimize possible lithium evaporation during reaction, large pellets (1 cm high, 2 cm diameter ⇒ large volume/surface ratio) were pressed. Solid-state reaction was performed twice, interrupted by an intermediate grinding, and pressing of new pellets. To approach equilibrium, long reaction times were chosen (2 × 2 days at 800 °C, 2 × 4 days at 700 °C, 2 × 7 days at 550 °C, 2 × 14 days at 400 °C). All pellets were quenched to liquid N_2. The 400 °C samples did not reach equilibrium. Lattice constants were obtained from Rietveld refinements. Table 4 gives the results.

Figure 22 shows the data of Table 4. Apparently, all single-phase samples for a given temperature lie on a straight line. All lines have the same slope. No deviation from linear behavior can be seen for any point obtained from single-phase spinel. Especially no deviation at the lower stability line (the most left data points) is visible. This clearly proves that cubic spinel above 400 °C is cation-mixed spinel. A small discrepancy between Figure 2 and Figure 22 exists. The data in Figure 2 overestimate the lithium stoichiometry by approximately 5%. The data of Figure 22 are more exact, and agree well with those of ref 22.

The data point for $T = 880$ °C lies slightly above the lines at lower temperature. This could indicate a slight oxygen deficiency. [Note that $LiMn_2O_4$ is stoichiometric for Li and Mn. Therefore, oxygen deficiency in principle is possible.] Assuming that the lattice constant is almost a function of the Mn oxidation state only allows an estimate of the oxygen deficiency $\delta = 0.027$ in $LiMn_2O_{4-\delta}$ at 880 °C. Since 880 °C is the upper stability limit of cubic spinel, this value is the upper limit for the oxygen deficiency. It coincides very well with the upper limit, $\delta < 0.025$, obtained from the SEC measurements.

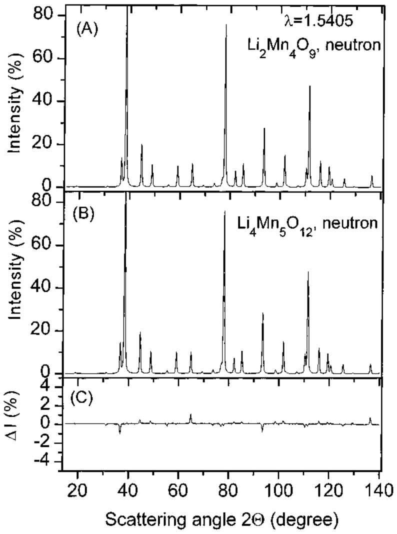

Figure 23. Calculated neutron diffraction profiles for $Li_2Mn_4O_9$ (panel A) and $Li_4Mn_5O_{12}$ (panel B) and their difference (panel C).

Cation-Deficient Spinel. The oxygen-rich phase or cation-deficient spinel phase $Li_2Mn_4O_9$ has been mentioned several times by Thackeray et al.[17,18] They prepared this phase at 400 °C in air. However, they mentioned "...loss of oxygen from $Li_2Mn_4O_9$ occurs when longer reaction times are used".[17] It is quite likely that Li_2MnO_9 is a metastable phase at 400 °C in air. Unfortunately, it is hard to distinguish $Li_2Mn_4O_9$ and $Li_4Mn_5O_{12}$ by either X-ray or neutron diffraction methods. Figure 23 shows calculated neutron diffraction patterns for the two phases, and their difference, using literature atom positions.[17] Even the best Rietveld analysis could not clearly distinguish the two patterns since the average Bragg peak intensity difference is less than 1%.

$Li_2Mn_4O_9$ is a member of the "cation-deficient" spinel solid−solution $Li_{1-x}Mn_{2-2x}O_4$ with $x = 1/9$. Cation-deficient spinels would have manganese as well as lithium vacancies. Our results clearly contradict the existence of this "double vacancy" solid−solution. (Single-phase spinel with Li:Mn = 1:2 was only achieved as stoichiometric $LiMn_2O_4$ above 800 °C.) Alternatively, $Li_2Mn_4O_9$ could also be understood as a member of the $\nu = 4$ line $Li_4Mn_5O_{12}-MnO_2$. Our results showed that only $Li_4Mn_5O_{12}$ (cation-mixed spinel) and $LiMn_{1.75}O_4$ (manganese-deficient spinel) is stable on this line. Notice that $Li_4Mn_5O_{12}$ is spinel without vacancies. $Li_1Mn_{1.75}O_4$ has Mn vacancies but is stoichiometric for lithium and oxygen. All other spinels with manganese oxidation state $\nu = 4$ exhibit more kinds of vacancies. This appears unlikely. We did not expect and did not observe such "multivacancy spinels".

Applications of the Phase Diagram. Figure 2 shows the lattice constant and T_{c1} of spinel

---

[22] Rousse, G.; Masquelier, C.; Rodriguez-Carvajal, J.; Hervieu, M. *Electrochem. Solid-State Lett.* **1998**, *2*, 6.

$Li[Li_xMn_{2-x}]O_4$ as a function of lithium stoichiometry x. T_{c1} is a straight line over the whole stoichiometry range whereas the lattice constant shows a deviation from linearity at $x = 0$. A discussion of this discrepancy is necessary since the relations $a(x)$ and $T_{c1}(x)$ have been suggested as tools to measure the lithium stoichiometry in spinel. The sample with $x = 0$ was prepared at 750 °C.[5] This temperature is below the lower stability line of stoichiometric spinel. Spinel with $x \cong 0.05$ is stable at this temperature. The true phase composition is probably spinel $Li[Li_{0.05}Mn_{1.95}]O_4 + 0.025Mn_2O_3$. This is confirmed by the lattice constant data. The point for $x = 0$ has a lattice constant $a \cong 8.24$ Å which corresponds to a spinel with $x \cong 0.05$.

The reason that T_{c1} misleads us to conclude that $x = 0$ is the back reaction proceeding during the TGA above 750 °C, that is, $Li[Li_{0.05}Mn_{1.95}]O_4 + 0.025Mn_2O_3 \Rightarrow 1.05LiMn_2O_4 + 0.0375O_2$. The measured T_{c1} is the T_{c1} of the spinel that consumed all Mn_2O_3. The deviation from linearity in Figure 2 leads to two conclusions. First, it proves the suggested phase diagram at 750 °C. Second, it displays the fact that the lattice constant is a measure of the lithium stoichiometry of the spinel phase whereas T_{c1} only gives the correct lithium stoichiometry if the material is single-phase spinel or if the impurity is Li_2MnO_3.

Spinel with a given cationic Li:Mn ratio has an upper and a lower stability temperature. If spinel has an oxygen stoichiometric range, then spinel at the upper stability limit will be oxygen deficient compared with spinel at the lower limiting temperature. The oxygen stoichiometry range δ, however, is negligible for cation-mixed spinels $Li_{1+x}Mn_{2-x}O_{4-\delta}$ ($x > 0$) and reaches a maximum of $\delta \cong 0.025$ for $Li_1Mn_2O_4$.

An extrapolation of the data in Figure 10 indicates that it is possible to prepare stoichiometric spinel at 400 °C if the oxygen partial pressure is $\cong 10^{-8}$ atm. If such pressures could be prepared, then in this way stoichiometric spinel with small crystallites could be prepared.

The phase diagram is very useful to understand properties of spinel after different preparations. One example out of many will be suggested. Quenched spinel $LiMn_2O_4$ fades more rapidly than spinel that was cooled slowly. During the cooling the lower stability line is crossed. During slow cooling a phase separation starts on the surface of the particle. Therefore, the surface of each particle will be covered by a thin layer of lithium-rich spinel $Li_{1+x}Mn_{2-x}O_4$, which could enhance the chemical stability of the surface in contact with the electrolyte.

CM9900960